Journal of Colloid and Interface Science 584 (2021) 610–621

Contents lists available at ScienceDirect

Journal of Colloid and Interface Science

journal homepage: www.elsevier.com/locate/jcis

Regular Article

Molecular dynamics simulations of the colloidal interaction between smectite clay nanoparticles in liquid water

Xinyi Shen [a,*], Ian C. Bourg [a,b]

[a] Department of Civil and Environmental Engineering, Princeton University, Princeton, NJ 08544, USA
[b] High Meadows Environmental Institute, Princeton University, Princeton, NJ 08544, USA

GRAPHICAL ABSTRACT

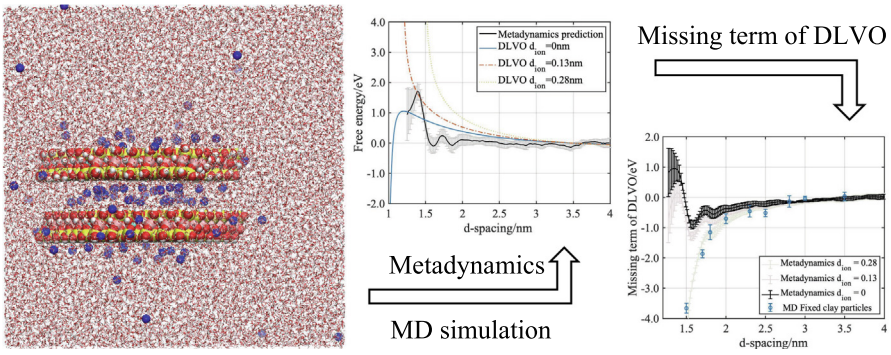

ARTICLE INFO

Article history:
Received 12 April 2020
Revised 20 August 2020
Accepted 8 October 2020
Available online 13 October 2020

Keywords:
Molecular dynamics simulation
DLVO theory
Clay swelling
Disjoining pressure
Adsorption
Electrical double layer
Colloidal aggregation

ABSTRACT

Colloidal interactions between clay nanoparticles have been studied extensively because of their strong influence on the hydrology and mechanics of many soils and sedimentary media. The predominant theory used to describe these interactions is the Derjaguin-Landau-Verwey-Overbeek (DLVO) model, a framework widely applied in colloidal and interfacial science that accurately predicts the interactions between charged surfaces across water films at distances greater than ~ 3 nm (i.e., ten water monolayers). Unfortunately, the DLVO model is inaccurate at the shorter interparticle distances that predominate in most subsurface environments. For example, it inherently cannot predict the existence of equilibrium states wherein clay particles adopt interparticle distances equal to the thickness of one, two, or three water monolayers. Molecular dynamics (MD) simulations have the potential to provide detailed information on the free energy of interaction between clay nanoparticles; however, they have only been used to examine clay swelling and aggregation at interparticle distances below 1 nm. We present the first MD simulation predictions of the free energy of interaction of smectite clay nanoparticles in the entire range of interparticle distances from the large interparticle distances where the DLVO model is accurate (>3 nm) to the short-range swelling states where non-DLVO interactions predominate (<1 nm). Our simulations examine a range of salinities (0.0 to 1.0 M NaCl) and counterion types (Na, K, Ca) and establish a detailed picture of the breakdown of the DLVO model. In particular, they confirm previous theoretical suggestions of the existence of a strong non-DLVO attraction with a range of ~ 3 nm arising from specific ion-clay Coulomb interactions in the electrical double layer.

* Corresponding author.

https://doi.org/10.1016/j.jcis.2020.10.029
0021-9797/

1. Introduction

How do charged surfaces attract or repel each other across thin fluid films? This core conundrum in interfacial science has vast implications across a number of disciplines [1–7]. In the natural sciences, for example, it determines the couplings between aqueous chemistry and mechanics in systems as diverse as aerosols, colloidal suspensions, biological cells, and sedimentary rocks [4,5,8–13].

A key framework in studies of the interactions outlined above is the well-known Derjaguin-Landau-Verwey-Overbeek (DLVO) model [3,14–17]. On this model, the swelling (or disjoining) pressure Π between parallel charged surfaces across a fluid film is approximated as the sum of van der Waals and osmotic contributions:

$$\Pi = P_{vdW} + P_{osm} \quad (1)$$

For solid surfaces separated by a water film, the van der Waals term is generally attractive and can be modeled as

$$P_{vdW} = -A/6\pi h^3 \quad (2)$$

where A is the Hamaker constant, which reflects the difference between solid–solid and solid-water London dispersion interactions, and h is the thickness of the film. The osmotic term is repulsive and routinely modeled by applying Van't Hoff's law between bulk liquid water and the pore mid-plane, where ion concentrations are determined by solving the Poisson-Boltzmann (PB) equation. For symmetrical 1:1 electrolytes, this yields:

$$P_{osm} = 2RTC_0(\sinh y - 1) \quad (3)$$

where C_0 is the concentration of the bulk solution, R the ideal gas constant, T absolute temperature, and y the reduced electrostatic potential at the pore mid-plane. To a first approximation, Eq. (3) simplifies to $P_{\mathrm{osm}} \propto 1/h^2$ as shown long ago by Langmuir [1]. A notable prediction of the DLVO model is that for charged solids separated by a thin water film, the balance between osmotic repulsion ($\propto 1/h^2$) and van der Waals attraction ($\propto 1/h^3$) results in the existence of a critical pore width below which the surfaces should snap to contact.

Beyond the well-established successes of the DLVO model, the principal limitation of the model is its reliance on the mean field approximation, i.e., it neglects specific interactions between ions, surface sites, and water molecules. Comparisons with experimental data suggest that this approximation is appropriate for water films thicker than ~3 nm but becomes increasingly inappropriate at shorter distances [16,18–22]. The breakdown of the DLVO model is most obvious for water films thinner than about 1 nm, where disjoining pressures display strong repulsion or oscillations with characteristic length scales commensurate with the thickness of a water monolayer (0.3 nm) [4,23–26]. In an effort to capture these observations, the right side of Eq. (1) is sometimes supplemented with a phenomenological 'hydration repulsion' term: [27,28]

$$P_{hyd} = Be^{-h/\lambda} \quad (4)$$

where B and λ are empirical parameters.

Efforts to validate and refine the equations outlined above have relied predominantly on two types of datasets: first, data on the forces across thin water films between atomically-smooth macroscopic surfaces obtained using surface force apparatus (SFA) and atomic force microscopy techniques (AFM) [3,29–34] and, second, data on the microstructure and swelling pressure in colloidal suspensions obtained using X-ray diffraction (XRD), cryogenic transmission electron microscopy (cryo-TEM), small-angle X-ray scattering (SAXS), transmission X-ray microscopy (TXM), and oedometric techniques [21,35–40]. An important reference surface for these experiments is the atomically-smooth basal surface of 2:1 layer-type phyllosilicate minerals. This surface is shared in particular by two classes of minerals, micas and smectites, that are widely used in SFA and AFM measurements [30,31,41–43] and in studies of colloidal interactions, [2,6,44–49] respectively. Beyond the importance of this surface in interfacial science, smectite nanoparticles are one of the most abundant constituents of soils and sedimentary rocks and their colloidal interactions often control fluid flow in these media, with important implications in soil science, contaminant hydrology, and energy geoscience [50–54].

An additional notable feature of the smectite-water system is that the breakdown of the DLVO model at short interparticle distances has been extensively documented in this system. Experimental studies established long ago that Eqs. 1–3 accurately describe smectite swelling at interparticle distances h > 2.5 nm, in the so-called *osmotic swelling* regime that predominates when uncompacted smectite is equilibrated with relatively dilute aqueous solutions (<0.2 M) containing predominantly Na counterions [2,21,35,47,55,56]. In other conditions including higher salinities, significant confining stresses, low relative humidities, or in the presence of Ca or K counterions, smectite nanoparticles exhibit a step-wise *crystalline swelling* with stable states at h = 0.3, 0.6, and 0.9 nm (the so-called one-, two-, and three-layer hydrates) that is not predicted by the DLVO model [36,38,40,47,55,56]. Theoretical models of the crystalline swelling regime remain sparse and tend to represent it as a series of discrete chemical or phase transition reactions [49,57,58]. Finally, the transition between the crystalline and osmotic swelling regimes (i.e., h values ranging from 0.9 to 2.5 nm) remains almost entirely unexamined because of the absence of stable swelling states in this range of interparticle distances.

Over the last decade, molecular dynamics (MD) simulations have emerged as an important tool to gain atomistic-level insight into colloidal interactions across thin water films [59–61], including between parallel smectite clay particles [62–68]. Because of the high computational cost of these simulations, the few studies that have examined the free energy of interaction of clay particles in liquid water focused on interparticle distances below 1 nm in a narrow range of aqueous chemistry conditions.

In the present study, we use MD simulations to examine the swelling energetics of a pair of parallel smectite clay nanoparticles suspended in bulk liquid water. We determine the free energy of swelling for a range of salinities (0 to 1.0 M NaCl) and exchangeable cation types (Na, K, Ca in 0.1 M Cl electrolytes) over a range of interparticle distances that includes the full transition from crystalline to osmotic swelling (h = 0.3 to 3.0 nm). We analyze our results to identify key controls on the free energy of swelling. In particular, we demonstrate the existence of a relatively long-ranged (~3 nm) non-DLVO attractive interaction arising from specific ion-clay Coulomb interactions in the EDL. We show that this interaction plays a key role in the breakdown of the DLVO model at interparticle distances below 3 nm.

2. Methodology

2.1. Molecular dynamics simulation

All-atom MD simulations were carried out on the Cori supercomputer at the National Energy Research Scientific Computing Center (NERSC) using the code LAMMPS [69] with the Colvars plugin [70]. The simulated systems consisted of two parallel hexagonal smectite nanoparticles surrounded by bulk liquid water in a cubic simulation cell with initial dimensions of 10 nm × 10 nm × 10 nm (total of about 100,000 atoms; Fig. 1a). The two nanoparticles had a unit cell formula $Si_8(Al_{3.2}Mg_{0.8})$

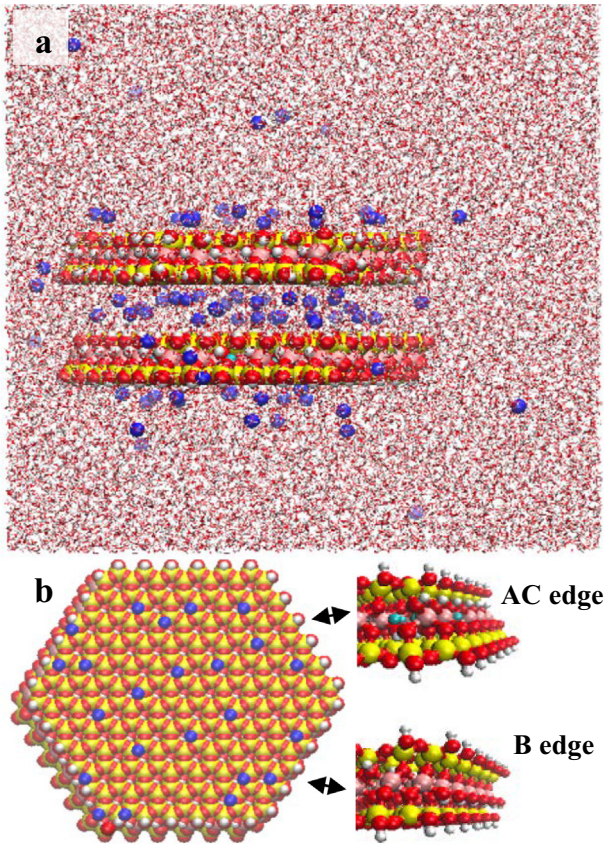

Fig. 1. Snapshot of a simulated system showing two parallel hexagonal Na-smectite nanoparticles surrounded by pure liquid water. Clay Si, Al, Mg, O, and H atoms are shown as yellow, pink, green, red, and white spheres. Sodium ions are shown as blue spheres. Water molecules are shown as red and white sticks. The lower panel highlights the hexagonal shape of the clay particles and their edge surface structures. (For interpretation of the references to colour in this figure legend, the reader is referred to the web version of this article.)

$O_{20}(OH)_4$ characteristic of montmorillonite, the prototypical dioctahedral smectite [71]. Each clay particle contained 54 effective unit cells and had a diameter of ~6 nm. For each clay particle, six stable uncharged edges were cleaved along crystallographic orientations thought to yield the most stable edge faces (the AC and B edges in the terminology introduced by White and Zelazny) [72] and healed with -OH and -H groups to mimic near-neutral pH condition (Fig. 1b). [68,73,74] Details on the structure of the edges are provided in the Supporting Information. Isomorphic substitutions of Al by Mg (90 substitutions in total) were randomly distributed in the smectite structure, yielding a mean basal surface charge density of -0.144C m^{-2}. Exchangeable cations (Na, K, or Ca) were placed on the smectite basal surface to balance the negative structural charge. Additional ions were added in solution as NaCl, KCl, or $CaCl_2$, respectively, to create aqueous solutions with 0.0, 0.1, 0.2, 0.5, or 1.0 M Cl concentration. These ions were initially evenly dispersed in the entire solution, including in the interlayers. Interatomic interactions were described using the SPC/E water model, [75] the CLAYFF model for smectite, [76] the Smith-Dang model for chloride, sodium, and potassium, [77,78] and the Åqvist model for calcium. [79,80] This combination of interatomic potential parameters has been extensively validated against the behavior of water and solutes on the surfaces of smectite, mica, and other silicate minerals. [68,81–85]

To obtain the free energy of swelling, we used the metadynamics technique, a steered MD simulation methodology capable of reconstructing complex free energy landscapes. [86,87] Briefly, this technique regularly adds small increments of positive biasing potential to the energy landscape defined by one or several predefined collective variables (i.e., reaction coordinates) to discourage the system from returning to previously explored states. This allows the system to escape local free energy minima and sample unfavorable states. [88] The simulations presented here used a single collective variable, the *d*-spacing of the parallel clay particles (i.e., the sum of particle thickness, 0.94 nm, and pore width *h*). The *d*-spacing was calculated as the distance between the centers of mass of the two clay particles. The lower clay particle was fixed, and the upper clay particle was allowed to move only in the *z* direction (no rotation or *xy* translation). During the metadynamics simulations, the biasing potential was incremented by addition every picosecond of a positive Gaussian potential of height 0.01 eV and width 0.2 Å. The Gaussian biasing potential was evenly distributed over all atoms in the two clay particles (>4000 atoms) such that the impact of each increment in biasing potential on any individual atom was<10^{-5} eV.

Each simulated system was equilibrated in the NVE ensemble for 50 ps with both clay particles fixed, followed by 2.1 ns in the NPT ensemble at 298 K and 0 bar. During the NPT ensemble simulation, the lower particle was fixed while the upper particle was allowed to move only in *z* direction. Finally, metadynamics simulations were carried out in the NPT ensemble at 298 K and 0 bar. The (cubic) simulation cell size was 103.0 ± 0.1 Å during the simulations. Water molecules were modeled as flexible using CLAYFF parameters. We note that due to the CLAYFF convention that atoms separated by an angle interact through both bonded and non-bonded interactions, our flexible SPC/E water model had a static dielectric constant about 25% lower than that of the rigid SPC/E model, though still within the range of existing water models. [89,90] Interatomic interactions were resolved in real space up to a distance of 12.0 Å. Long-range Coulomb interactions beyond 12.0 Å were resolved in reciprocal space using the particle–particle/particle-mesh (PPPM) technique with 99.99% accuracy.

2.2. Metadynamics simulation details

To the best of our knowledge, no previous study has used metadynamics to examine swelling in colloidal systems. In the case of smectite, existing all-atom simulation predictions of swelling free energy have relied on a number of techniques including MD simulations of an infinite stack of clay layers in the $\mu_{H2O}VT$ ensemble, where the swelling pressure was determined using the trial volume method, then integrated to obtain the swelling free energy; [62,66] simulations of a pair of rigid clay nanoparticles surrounded by bulk liquid water in the NVT ensemble, where the free energy of swelling was determined by applying free energy perturbation theory between systems with different interparticle distances; [63] and simulations of a pair of flexible clay nanoparticles in bulk liquid water in the NPT ensemble, where the free energy of swelling was determined using umbrella sampling. [91] A few other studies have used methodologies that yield the swelling pressure but do not enable a precise determination of the swelling free energy. [64,67] A potentially useful feature of the metadynamics methodology, relative to the methods outlined above, is that it enables examining free energy along several reaction coordinates simultaneously; [92] this possibility was not utilized here but may be explored in future studies.

A key challenge associated with the use of metadynamics is that the accuracy of simulation predictions can be sensitive to the rate of addition of biasing potential. Slower rates of bias addition can require very long simulation times, particularly in systems with vast free energy landscapes or deep free energy minima. Conversely, faster rates of bias addition can cause artifacts (e.g., inaccurate buildup of bias in a given location) if the rate of bias

addition is too rapid relative to the time-scale on which the system reacts to the evolving (biased) free energy landscape. This challenge is particularly acute in the present study, because the slow Brownian diffusion of the clay particles causes them to explore the evolving free energy landscape relatively slowly. To alleviate this issue, we carried out six parallel simulations at each aqueous chemistry condition of interest; in each of these simulations, the system was constrained to explore prescribed, partially-overlapping 9-Å-wide ranges in interparticle distance with *d*-spacings ranging from 8 to 42 Å. To restrain the clay particles to the desired range of *d*-spacings, we used one-sided harmonic biasing potentials at the edges of the desired range. [70] After determining the free energy profile in each 9-Å-wide interval in *d*-spacing, we combined the six profiles into a single free energy profile from 8 to 42 Å based on the continuity of the free energy in the 4-Å-wide regions where neighboring profiles overlapped. For each simulated system, we carried out 55 ns of metadynamics simulations in the NPT ensemble as described in the previous section and calculated the average free energy profile for each segment by averaging the profiles reported every 1 ns during the last 35 ns of each simulation. [87] We calculated 95% confidence intervals on the resulting average free energy profiles based on an estimate that the 35 averaged profiles represent roughly seven independent observations. Additional details of our metadynamics simulation methodology are provided in the Supporting Information.

2.3. MD simulations at fixed d-spacing

In addition to the metadynamics simulations described above, standard MD simulations were carried out in the NPT ensemble (298 K, 1 bar) for 5 ns with smectite nanoparticles constrained to fixed *d*-spacings of 1.2, 1.5, 1.7, 1.8, 2.0, 2.3, 2.5, 3.0, or 3.5 nm in solutions with different aqueous chemistries. Output trajectories were analyzed during the final 4 ns of these simulations to determine the average density profiles of water and ions in the direction normal to the surfaces for comparison with the predictions of the PB equation. To minimize the influence of clay edges, these density profiles were calculated within 1.5 nm of the axis of symmetry of the stack of clay particles.

Simulation results at fixed *d*-spacing also were analyzed to quantify the impact of specific ion-ion, ion-clay, and clay-clay Coulomb interactions on clay swelling. Specifically, we calculated the average potential energy associated with these interactions ($E_{\text{pot,ion-ion}}$, $E_{\text{pot,ion-clay}}$, $E_{\text{pot,clay-clay}}$) as a function of *d*-spacing. These potential energies, as directly calculated by LAMMPS using Coulomb's law, do not account for dielectric screening by water and clay. Therefore, we also calculated the average static dielectric constant within the stack of clay particles using the appropriate relation for systems simulated using a standard Ewald sum treatment of long-range interactions: [93–96]

$$\epsilon = 1 + \left[\frac{< M^2 > - < M >^2}{3\epsilon_0 V k_B T}\right] \tag{5}$$

In Eq. (5), ϵ_0 is the permittivity of vacuum (8.854×10^{-12} F m^{-1}), k_B is Boltzmann's constant (1.381×10^{-23} J K^{-1}), V is the volume of the region of interest (here a cylinder located on the axis of symmetry of the clay stack, with a height equal to the *d*-spacing and a radius of 1.5 nm), and M is the total dipole moment in the region of interest, approximated as the sum of the dipole moments μ_i of all water molecules in this region: [97]

$$M = \sum_{i=1}^{N} \mu_i \tag{6}$$

Finally, simulations at fixed *d*-spacing were analyzed to evaluate the importance of ion and surface hydration effects, specifically by quantifying the potential energy associated with water-ion and water-clay interactions ($E_{\text{pot,water-ion}}$, $E_{\text{pot,water-clay}}$) as a function of *d*-spacing.

2.4. Mean field theory prediction of EDL structure and P_{osm}

For comparison with our MD simulation results, we derived a mean field theory prediction of the structure of the EDL and the contribution of osmotic phenomena to the free energy of swelling as prescribed by the DLVO model. Details are provided in the Supporting Information. Briefly, we predicted the electrostatic potential profile between infinite parallel clay particles by solving the PB equation in the *z* direction. [98–100] The osmotic pressure caused by the difference between the average ion concentration in the bulk aqueous solution and at the midplane of the interlayer nanopore was then calculated using Eq. (3). The predicted osmotic contribution to the free energy of swelling was obtained by integrating P_{osm} as a function of inter-particle distance: [101]

$$\Delta G_{osm} = -A \int P_{osm} dz \tag{7}$$

3. Results

3.1. Water and ion density profiles near Na-smectite particles as a function of salinity

Water and ion density profiles predicted from our MD simulations of Na-smectite at a fixed *d*-spacing of 3.0 nm in a 0.1 M NaCl aqueous solution are reported in Fig. 2. A selection of results obtained at other salinities and other *d*-spacings is provided in the Supporting Information. As shown in Fig. 2, water density profiles exhibit three peaks as a function of distance from the surface: a sharp density peak located 3.33 ± 0.25 Å from the plane of surface O atoms followed by less pronounced peaks located 6.84 ± 0.16 and 9.44 ± 0.16 Å away. The spacing between these peaks (3 ± 0.5 Å) is consistent with previous SFA, AFM, XRD, and MD simulations studies indicating the existence of three ordered water monolayers at the clay-water interface. [20,47,102] Water density profiles obtained at different salinities are essentially identical, suggesting that short-range hydration repulsion effects are likely invariant with salinity.

Predicted Na and Cl density profiles (blue lines) reveal the existence of an EDL where the negative surface charge of the clay par-

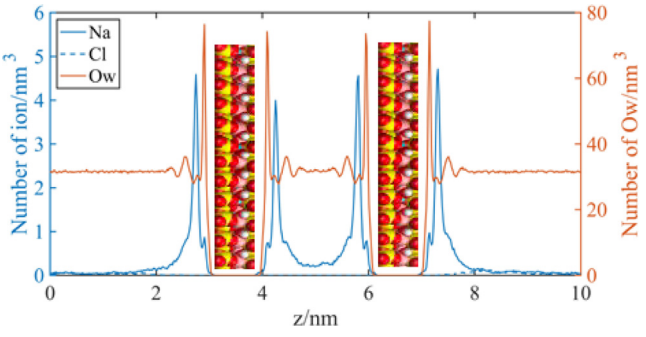

Fig. 2. Water O, Na, and Cl density profiles (red, solid blue, and dashed blue lines) in the direction normal to the clay basal surface during simulations with a fixed *d*-spacing of 3 nm (i.e., pore width h = 2.06 nm) at a salinity of 0.1 M NaCl. Results at other salinities are shown in the Supporting Information. (For interpretation of the references to colour in this figure legend, the reader is referred to the web version of this article.)

ticles is screened by cation adsorption and anion repulsion. [50,103,104] In agreement with previous studies, Na ions form three types of adsorbed species at the smectite-water interface: inner- and outer-sphere surface complexes and a diffuse ion swarm. [105,106] On the external basal surfaces, Na and Cl densities become essentially identical at distances from the surface greater than ~1 nm, indicating the existence of bulk-liquid-like water. In the interlayer nanopore, in contrast, Na density exceeds Cl density everywhere in the pore if salinity is sufficiently low and the pore is sufficiently narrow. Within the framework of the PB equation, this implies that the electrostatic potential y is negative everywhere in the pore, i.e., the EDLs on opposite clay surfaces overlap at the pore mid-plane. According to Eq. (3), this should give rise to a repulsive osmotic swelling pressure.

3.2. Ion density profiles near Na-smectite clay particles as a function of interparticle distance

The impact of interparticle distance on the sodium density profile is illustrated in the case of Na-smectite in pure water in Fig. 3. On the external basal surface (left side of Fig. 3), the sodium density profile is invariant with interparticle distance and reveals the existence of inner-sphere, outer-sphere, and diffuse-layer species with peaks located 3.30 ± 0.16, 4.90 ± 0.16 and 6.83 ± 0.28 Å from the plane of surface O atoms (as also observed in Fig. 2). Within the interlayer nanopore (right side of Fig. 3), for interparticle distances beyond the 3-layer hydrate (i.e., d-spacing > 1.85 nm), a similar Na distribution is observed, but the sodium concentration does not decay to zero at the pore mid-plane. As noted above in the case of Fig. 2, this indicates that $y < 0$ everywhere in the pore, which should give rise to a repulsive osmotic swelling pressure. In the crystalline swelling regime (d-spacings $\leq$ 1.85 nm), the interlayer sodium density profile becomes increasingly distorted with the successive disappearance of diffuse layer Na at d-spacings $\leq$ 18 Å, then outer-sphere Na at d-spacings $\leq$ 15 Å.

3.3. Metadynamics predictions of the free energy of swelling: Signal vs. Noise

Predicted swelling free energy profiles are reported in Fig. 4 as a function of d-spacing (1.2 to 4.0 nm) for all simulated aqueous chemistry conditions. For each simulation, free energy is shown relative to the average value predicted for d-spacings between 3.5 and 4.0 nm.

The free energy profiles in Fig. 4 show evidence of significant statistical noise, as reported in other studies that used the metadynamics technique. [87,92,107] In particular, features observed at d-spacings > 2.0 nm are not consistently present at different aqueous chemistries. Furthermore, these features tended to attenuate with increasing duration of the metadynamics simulation. We infer that

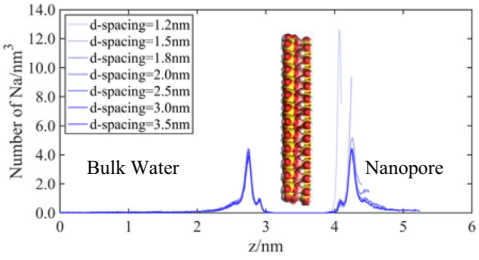

Fig. 3. Sodium density profiles in the direction normal to the clay basal surface during simulations of Na-smectite in pure water (0.0 M NaCl) at a range of fixed d-spacings. For clarity, Na density profiles are plotted only up to the mid-plane of the interlayer nanopore.

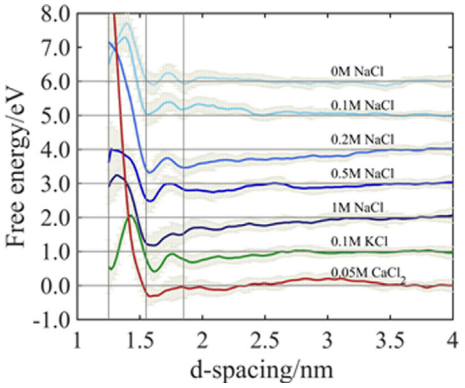

Fig. 4. Relative free energy of swelling as a function of basal spacing (i.e., the sum of particle thickness, 0.94 nm, and pore width h) for parallel smectite particles at different aqueous chemistry conditions. The three vertical lines show the expected d-spacings of the 1-, 2-, and 3-layer hydrates.

the free energy profiles are essentially featureless at d-spacings of 2.0 to 4.0 nm, in agreement with experimental results demonstrating the absence of stable swelling states in this range of interparticle distances.

At shorter interparticle distances (d-spacings < 2 nm), the profiles predicted at different aqueous chemistry conditions display significant systematic features and trends. In particular, almost all curves display local minima at d-spacings ≈ 1.25, 1.55, and 1.85 nm (vertical lines in Fig. 4) in agreement with previously reported values for the 1-, 2-, and 3-layer crystalline hydrates, respectively. [2,20,102,108,109]

Finally, at d-spacings > 2 nm, the essentially flat nature of the profile predicted for Na-smectite in pure water (the highest curve in Fig. 4) is consistent with observations that Na-smectite nanoparticles delaminate entirely in pure water. [110,111] Conversely, the upward sloping nature of the profile at higher salinities (most evident in the curves at 0.2 and 1.0 M NaCl) is consistent with the observed increased stability of the crystalline hydrates with increasing salinity. [2,40]

3.4. Free energy of swelling of Na-smectite at zero salinity: Comparison with previous atomistic simulations

Our metadynamics prediction of the swelling free energy of Na-smectite in pure water (the highest curve in Fig. 4) is reproduced in Fig. 5 with error bands reflecting statistical uncertainty at the 95% confidence level and compared with previous atomistic simulation predictions. [62,63,91] In the case of Whitley and Smith, [62] the free energy profile was calculated from the reported swelling pressure using Eq. (7).

As shown in Fig. 5, our predictions for the swelling of Na-smectite at zero salinity are in excellent agreement with the results of Whitley and Smith. [62] Our results also are broadly consistent with those of Ho et al, [91] the main differences being a minor (~0.1 nm) offset in d-spacing and the unexpected absence of a minimum at the d-spacing of the 1-layer hydrate in Ho et al. [91] (discussed in detail in their study). We note that the profile by Ho et al. [91] shown in Fig. 5 was obtained using a slightly modified version of the CLAYFF interatomic potential model designed to more accurately predict the stability of the 0-layer hydrate; their simulations using the original CLAYFF model (shown in the Supporting Information of their paper) yielded a local minimum for the 1-layer hydrate consistent with our results. Finally, the results of Ebrahimi et al. [63] as originally reported cannot possibly be correct: they display free energy maxima at the well-known locations of free energy minima (i.e., the d-spacings of the 0-, 1-, 2-, and 3-layer

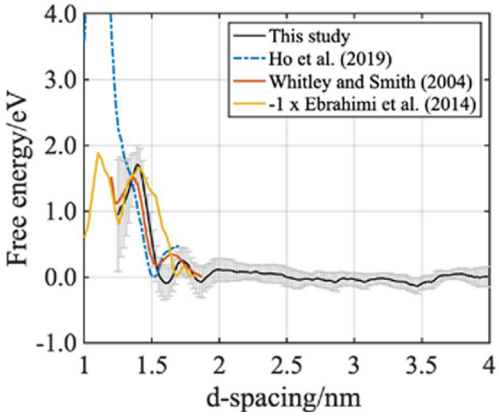

Fig. 5. Comparison with the three previous all-atom simulation predictions of the free energy of swelling of Na-smectite in pure water. Our prediction (black line) is replotted from Fig. 4 and displayed with error bands that reflect statistical uncertainty. The four free energy profiles are consistent with experimental observations of the existence of one-, two-, and three-layer hydrates with *d*-spacings of ≈ 1.25, 1.55, and 1.85 nm.

hydrates). They are, therefore, inconsistent with the entire, vast experimental database on clay swelling as well as with the three other modeling datasets shown in Fig. 5. We note, however, that the results reported by Ebrahimi et al. [63] are essentially a mirror image of the three other simulation datasets. Rather than discard them, we report them in Fig. 5 with a simple scaling factor of −1 that reconciles them with all other experimental and simulation studies. A modified version of Fig.5 without this scaling factor is provided in the Supporting Information.

Overall, the four datasets are remarkably consistent despite their use of four distinct methodologies to reconstruct the free energy landscape as noted in the introduction. Further methodological distinctions between the four studies include differences in structural charge density (0.75 to 0.8 e per unit cell), isomorphic substitution type (either predominantly [63] or entirely in the octahedral layer), and interatomic potential models [CLAYFF and SPC in Ebrahimi et al.; [63] CLAYFF and SPC with revised Na-Oclay interaction parameters in Ho et al.; [91] CLAYFF and flexible SPC/E in the present study; a modified version of the clay force field of Skipper et al [82] combined with SPC/E water in Whitley and Smith]. [62] In addition to providing confidence in our simulation predictions, Fig. 5 highlights the wider range of interparticle distances (and also of aqueous chemistry conditions, since previous studies focused on pure water) examined here relative to previous MD simulation studies.

We note that our simulation results below 1.2 nm are not shown in Fig. 5 because of a clear artifact at sub-monolayer hydration levels, as described in the Supporting Information. The difficulty of predicting swelling free energy at sub-monolayer hydration is not inherent to our methodology: it was discussed by Ho et al. [91] and is further illustrated by the fact that Whitley and Smith [62] did not report results in this regime.

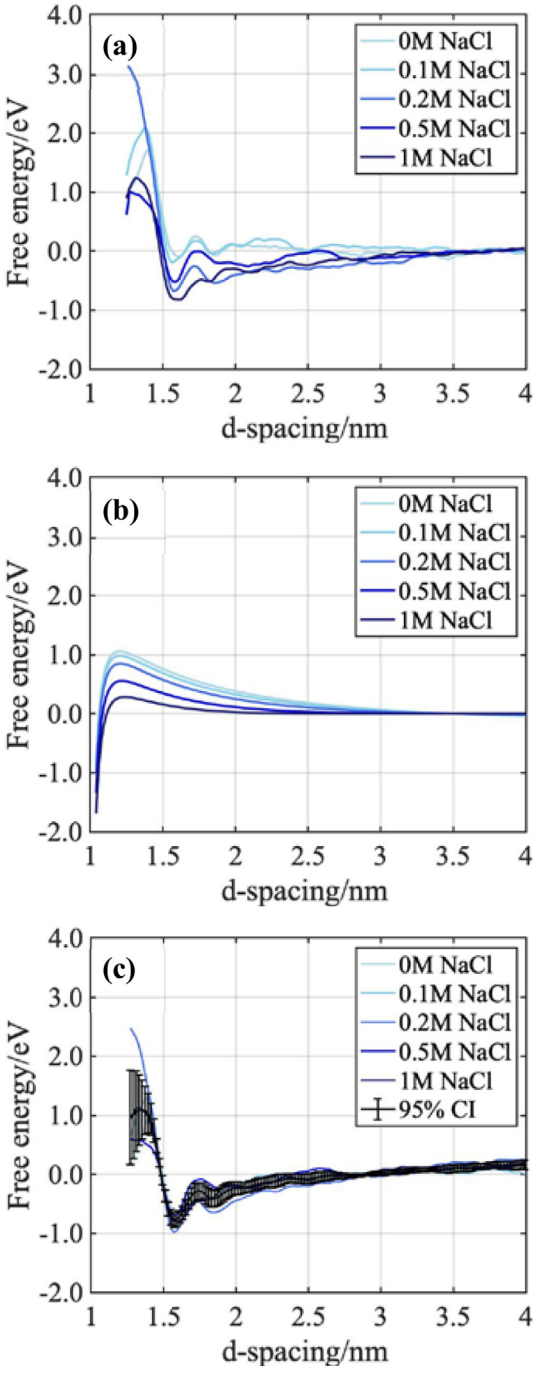

Fig. 6. Simulation predictions of the free energy of swelling of Na-smectite as a function of *d*-spacing at different NaCl concentrations: (a) metadynamics simulation prediction; (b) DLVO model prediction; (c) non-DLVO component. The DLVO prediction was corrected to account for the geometry of the simulated system (i.e., it accounts for interactions with both the neighboring particle and its periodic image and, hence, yields a minimum free energy at 5 nm).

3.5. Swelling of Na-smectite as a function of salinity (0.0 to 1.0 M NaCl) and comparison with the DLVO model

A systematic comparison of swelling free energy vs. *d*-spacing for two Na-smectite clay particles in solutions with different NaCl concentrations is presented in Fig. 6. Briefly, Fig. 6a shows our metadynamics simulation predictions, Fig. 6b shows the prediction of the DLVO model, and Fig. 6c shows our calculation of the non-DLVO component of the free energy of swelling. In Fig. 6c, we also report the average and 95% confidence interval of the profiles obtained at different salinities (black line).

As shown in Fig. 6a, crystalline swelling is increasingly favored with increasing salinity. This trend is qualitatively consistent with the experimental database. [2,36,40,112,113] It also is consistent with the DLVO model (Fig. 6b), suggesting that it reflects the processes represented by Eq. (3), i.e., osmotic uptake of water in the clay interlayer, driven by the excess ion concentration at the pore

mid-plane, combined with the attenuation of this excess at high salinities.

We note, in passing, that according to the DLVO model predictions in Fig. 6b, osmotic repulsion predominates over van der Waals attraction at *d*-spacings > 1.25 nm. In short, the van der Waals contribution to swelling free energy should be close to zero at all interatomic distances probed by our simulations.

To gain further insight into the free energy of interaction shown in Fig. 6a, we calculated its non-DLVO component as the difference between the curves in Fig. 6a and b. The results, shown in Fig. 6c, reveal that the non-DLVO component is relatively long-ranged (it extends to *d*-spacings of at least 3.5 nm), similar in magnitude to the DLVO component, and essentially invariant with salinity. In other words, interparticle interactions that are not captured by the mean field description of osmotic and van der Waals interactions in Eqs. (1)–(4) contribute significant attractive free energy at interparticle distances up to ~ 10 water monolayers. At pore widths h = 0.9 to 3 nm (i.e., at *d*-spacings of 1.85 to 3.95 nm, in the entire transition between the crystalline and osmotic swelling regimes), the two predominant contributions to the free energy of swelling are the DLVO osmotic repulsion and the non-DLVO attraction, as suggested by theoretical calculations [114,115] and classical DFT simulations. [116]

3.6. Sensitivity analysis of the DLVO model prediction

To gain insight into the accuracy of the DLVO model predictions in Fig. 6b, we examined the sensitivity of these predictions to the two main input parameters of the DLVO model: the Hamaker constant of the clay-water-clay system (A) and the distance of closest approach of ions to the clay-water interface (d_{ion}). For the first parameter, we tested three different values: a value of 22 zJ used in many studies of smectite swelling in water, [28,117] a value of 8 ± 1 zJ estimated in a recent study by Tester et al., [40] and an intermediate value of 15 zJ (Fig. 7a). For the second parameter, we tested three different values (d_{ion} = 0, 0.13, and 0.28 nm) that locate the plane of closest approach of ions to the clay surface either at the clay-water interface, at the main water density peak, or at the main Na density peak (Fig. 7b). Corresponding ions density profiles predicted using the PB equation with each of the three values of d_{ion} are shown in Fig. 7c in the case of Na-smectite in pure water with a *d*-spacing of 3 nm.

As shown in Fig. 7, our DLVO model predictions are sensitive to the choice of A at *d*-spacings up to ~ 1.5 nm and to the choice of d_{ion} at *d*-spacings up to ~ 2.5 nm. Therefore, the long-range non-DLVO attraction reported in Fig. 6c is sensitive to the value of d_{ion} used to obtain the DLVO model predictions in Fig. 6b. The model predictions in Fig. 6b were obtained using d_{ion} = 0 and A = 8 zJ. According to our sensitivity analysis, the results shown in Fig. 6c constitute a lower boundary on the magnitude of the long-range non-DLVO attraction. If d_{ion} > 0, this attractive non-DLVO interaction may be stronger by up to a factor of two.

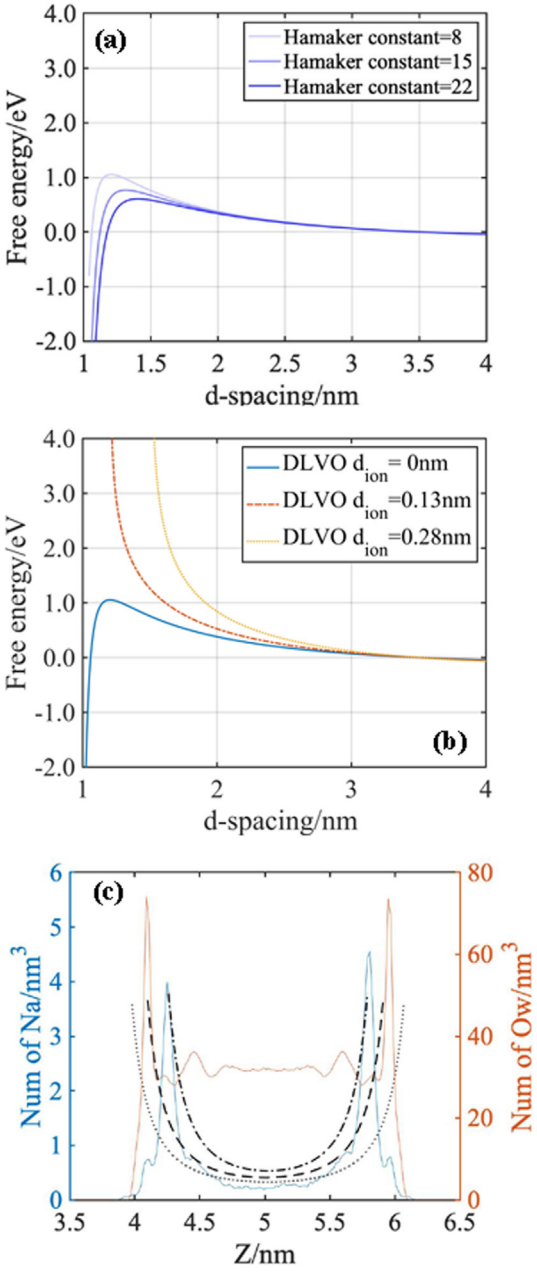

Fig. 7. Sensitivity analysis of the DLVO model prediction (Fig. 6b) in the case of Na-smectite in pure water. (a) Sensitivity to the clay-water-clay Hamaker constant (A = 8 to 22 zJ). (b) Sensitivity to the distance of closest approach of ions to the clay surface (d_{ion} = 0, 0.13, or 0.28 nm). (c) PB model prediction of the Na density profile within the interlayer nanopore calculated using d_{ion} = 0, 0.13, or 0.28 nm (black lines) compared with our MD simulation prediction (blue line); the water O density profile in the pore is also shown (red line). (For interpretation of the references to colour in this figure legend, the reader is referred to the web version of this article.)

3.7. Contribution of specific ion-ion, ion-clay, and clay-clay Coulomb interactions to the free energy of swelling

As noted in the introduction, a well-known limitation of DLVO theory is that it fails to account for specific charge-charge interactions in the EDL. [8,21,26,118,119,30] Various efforts have been carried out to evaluate these interactions including theoretical derivations [114,115,120] and classical DFT calculations. [116,121–123] To estimate the magnitude of this effect from our MD simulations, we use our results for Na-smectite in pure water at fixed *d*-spacings to calculate the total potential energy associated with ion-ion, ion-clay, and clay-clay Coulomb interactions (Fig. 8a). We also calculate the average dielectric constant within the stack of clay particles (Fig. 8b) as a function of *d*-spacing. Finally, we divide the (unscreened) potential energies in Fig. 8a by the dielectric constant in Fig. 8b to obtain a first-order estimate of the contribution of screened Coulomb interactions between charged species in the EDL to the free energy of swelling (Fig. 8c).

As shown in Fig. 8a, Coulomb interactions between charged species in the EDL (blue line) are overall favorable, i.e., clay-cation Coulomb attraction is greater than the sum of cation-cation and clay-clay repulsion. These interactions become even more favorable at smaller *d*-spacings, likely because of the compression of the EDL in the nanopore. If dielectric screening were

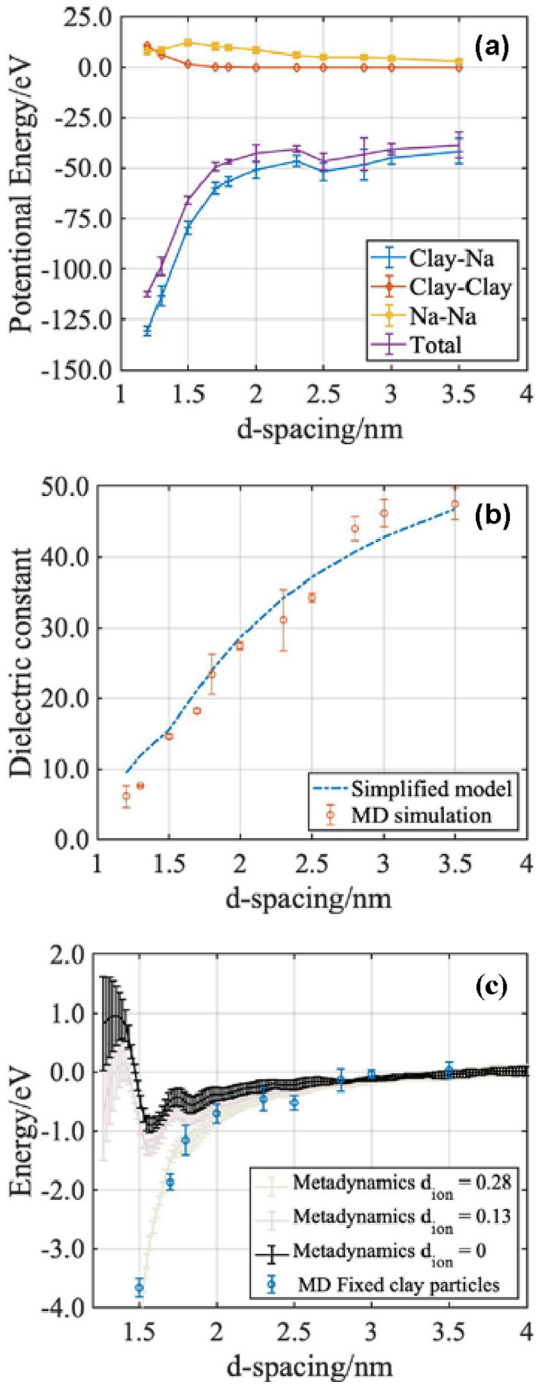

Fig. 8. Contribution of specific Coulomb interactions between charged species in the EDL to the free energy of swelling in the case of Na-smectite in pure water. (a) Potential energies $E_{pot,ion\text{-}ion}$, $E_{pot,ion\text{-}clay}$, and $E_{pot,clay\text{-}clay}$ as a function of *d*-spacing. (b) Average dielectric constant within the stack of clay particles (red symbols) and comparison with the simple parametric fit described in the text (blue curve); (c) Non-DLVO component of the free energy of swelling (black line from Fig. 6c; alternative predictions obtained using larger values of d_{ion} are shown as pale purple and green lines) and first-order estimate of the contribution from screened specific charge-charge interactions in the EDL (blue symbols). (For interpretation of the references to colour in this figure legend, the reader is referred to the web version of this article.)

invariant with *d*-spacing, these specific charge-charge interactions would result in a net attractive contribution to the free energy of swelling with a magnitude of ~1 eV at *d*-spacings between 1.2 and 2.0 nm (i.e., the difference in potential energy between 1.2 and 2.0 nm, ~70 eV, scaled by the static dielectric constant of bulk SPC/E water, 71), with only a minor effect at *d*-spacings >2.0 nm. The existence of such a non-DLVO attraction associated with specific charge-charge interactions in the EDL is consistent with theoretical calculations. [114,115]

A notable difference between our results and those reported in previous studies is that our simulations enable a rough accounting for the impact of nanopore width on dielectric screening. Our predicted ϵ-values obtained using Eq. (5) are shown as red symbols in Fig. 8b and compared with a parametric fit (blue curve) calculated as a weighted sum of ϵ-values in the clay particles (ϵ_{clay}), in the first water layer on the clay surface ($\epsilon_{1st-layer}$), and in subsequent water layers (ϵ_{water}). Specifically, the blue curve was obtained by imposing ϵ_{clay} = 1 and ϵ_{water} = 71 (the value for bulk liquid SPC/E water) [75,124] and adjusting the value of $\epsilon_{1st-layer}$ to minimize the root-mean-square difference with our MD predictions. This yields a value of $\epsilon_{1st-layer}$ = 40. In short, ϵ-values calculated from the configurations of interlayer water molecules can be modeled simplistically by assigning to the first water layer on each clay surface a dielectric constant equal to about half of that of bulk liquid water, in rough agreement with results reported in previous experimental and MD simulation studies. [125–128]

Finally, Fig. 8c shows the comparison between the non-DLVO component of the free energy of swelling reported in Fig. 6c and our first-order estimate of the contribution of screened specific Coulomb interactions between charged species in the EDL (i.e., the purple values in Fig. 8a scaled by the red values in Fig. 8b and adjusted to an arbitrary reference value of zero at a *d*-spacing of 3.5 nm). The two datasets are qualitatively consistent with regard to the overall shape of the non-DLVO contribution at *d*-spacings ranging from 1.55 to 3.5 nm. The difference between the two estimates (a factor of ~ 2 to 3 in the magnitude of the attractive interaction) is consistent with the expectation that the results shown in Fig. 6c may underestimate attraction by up to a factor of two, as noted above, because they are based on the DLVO calculation with d_{ion} = 0. Conversely, the blue symbols in Fig. 8c may tend to overestimate attraction, because they are based on the average dielectric constant within the stack of clay particles. Overall, Fig. 8a-c suggest that specific charge-charge Coulomb interactions in the EDL can explain most if not all of the attractive non-DLVO interaction at *d*-spacings > 1.5 nm.

3.8. Hydration repulsion

As noted in the previous section, at *d*-spacings > 1.5 nm the black line and blue symbols in Fig. 8c are qualitatively consistent. Quantitatively, they differ by a factor of ~ 2 that is commensurate with the sensitivity of the DLVO calculation to poorly-constrained parameters. At *d*-spacings < 1.5 nm, however, the two datasets predict qualitatively different behaviors: the black and pale purple curves show that dehydration below the two-layer hydrate must overcome a 1.5 to 2 eV free energy barrier (the pale green curve predicts that dehydration below the two-layer hydrate is impossible, as it assumes that ions cannot approach closer than 0.28 nm from the surface); conversely, the blue symbols predict increasingly attractive interactions at *d*-spacings below 1.5 nm (not shown in the figure). In short, whereas specific charge-charge Coulomb interactions in the EDL can explain most if not all of the attractive non-DLVO interaction at *d*-spacings > 1.5 nm, these interactions cannot predict the strong barrier to dehydration below the two-layer hydrate. This discrepancy is consistent with the expected existence of a strong short-range repulsion associated with surface and ion hydration effects (Eq. (4)). [129,130] A precise estimate of the magnitude of this hydration repulsion from our metadynamics results is unfortunately not possible, because our

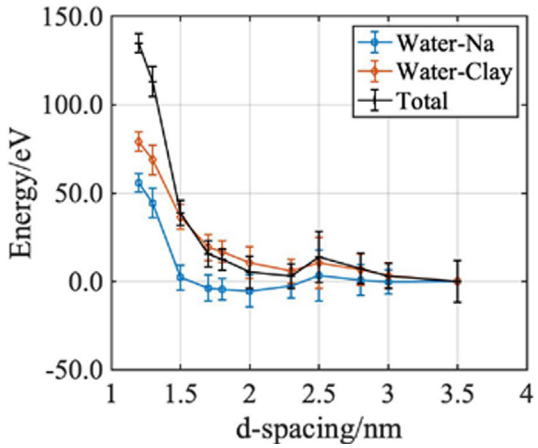

Fig. 9. Potential energies $E_{pot,water-ion}$, and $E_{pot,water-clay}$ as a function of *d*-spacing in the case of Na-smectite in pure water.

estimate of the non-DLVO component is highly sensitive to the choice of both d_{ion} and *A* at *d*-spacings < 1.5 nm.

Partial insight into the hydration repulsion effect is accessible, however, from the potential energies associated with water-Na and water-clay interactions during our MD simulations at fixed *d*-spacing. These potential energies are reported as a function of *d*-spacing in Fig. 9. A direct translation of these potential energies into a contribution to the free energy of swelling is not possible. Nonetheless, the results in Fig. 9 are consistent with the observation, based on Fig. 8c, that hydration repulsion effects play an important role at *d*-spacings < 1.5.

4. Summary

We present the first existing application of the metadynamics methodology to the evaluation of the free energy of interaction of colloidal particles. Despite the known limitations of the methodology (notably, the very long simulation times required to reduce statistical noise), our methodology is validated in three ways: first, our calculations at all salinities correctly predict the location of the free energy minima corresponding to the 1-, 2-, and 3-layer hydrates as extensively established in experimental studies of clay swelling. Second, our detailed prediction of the free energy of swelling of Na-smectite swelling in pure water is consistent with two of the three previous molecular simulation datasets as shown in Fig. 5. Third, although the free energy profiles obtained at different NaCl concentrations show significant statistical noise (Fig. 6a), these profiles collapse onto a single curve when the DLVO theory prediction is removed (Fig. 6c), which strongly suggests that statistical noise does not impact the overall accuracy of the results.

Our simulation results provide a detailed view of the free energy of swelling of smectite clay nanoparticles in a wide range of interparticle distances (pore widths *h* = 0.3 to 3.0 nm) as a function of salinity (0 to 1.0 M NaCl). Our results agree with experimental results, and previous atomistic simulation predictions of swelling free energy obtained in a much narrower range of conditions. At the same time, our results reveal an unexpected feature: the absence of a free energy barrier between the crystalline and osmotic swelling states.

Further analysis of our simulation results reveals that the breakdown of DLVO theory at interparticle distances < 3 nm in NaCl electrolytes is caused by a non-DLVO attractive interaction with a range of ~3 nm. This non-DLVO attraction is essentially invariant with salinity and obtains mostly or entirely from specific charge-charge Coulomb interactions in the EDL. At interparticle distances < 0.6 nm, our results also show evidence of a strong short-range non-DLVO repulsion associated with cation and surface hydration effects.

One implication of our results is that the free energy of swelling of smectite should depend on the extent of particle stacking, not only through its influence on the Van der Waals attraction terms (as noted previously) [21] but also through the potential influence of the degree of stacking on the static dielectric constant within the stack. This effect was not examined here but may represent an interesting avenue for future study.

The present analysis focused primarily on the swelling of Na-exchanged smectite as a function of salinity. Simulations using K and Ca cations (instead of Na) at a single salinity showed a strong inhibition of clay swelling, in agreement with experimental results. A more detailed examination of the influence of different organic and inorganic cations on clay swelling will be presented in future work.

Beyond the four components of the free energy of swelling examined here (van der Waals attraction, osmotic repulsion, specific charge-charge Coulomb attraction, and hydration repulsion), the influence of interparticle distance on the configurational entropy of colloidal particles is known to give rise to an additional attractive contribution in colloidal suspensions [120,131,132]. This effect was absent in the present study as the particles were constrained in a parallel orientation.

Finally, we note that the basal surface of Na-smectite is somewhat of a limiting case among charged surfaces in that it develops a very prominent EDL (i.e., only a small fraction of the surface charge is screened by inner-sphere surface complexes). For other charged surfaces where a significant fraction of surface charge is screened by inner-sphere surface complexes, the importance of both DLVO osmotic repulsion and the non-DLVO attraction examined here may be attenuated sufficiently that other contributions to the swelling free energy become important. [11,116].

CRediT authorship contribution statement

Xinyi Shen: Conceptualization, Methodology, Software, Formal analysis, Writing - original draft, Visualization. **Ian C. Bourg:** Conceptualization, Methodology, Software, Resources, Validation, Supervision, Funding acquisition, Writing - review & editing.

Declaration of Competing Interest

The authors declare that they have no known competing financial interests or personal relationships that could have appeared to influence the work reported in this paper.

Acknowledgments

This research was carried out under the auspices of the U.S. Department of Energy, Office of Science, Office of Basic Energy Sciences, Geosciences Program under Award DE-SC0018419. Molecular dynamics simulations were carried out using resources of the National Energy Research Scientific Computing Center (NERSC), which is supported by the U.S. Department of Energy, Office of Science, under Award DE-AC02-05CH11231.

Appendix A. Supplementary material

Supplementary data to this article can be found online at https://doi.org/10.1016/j.jcis.2020.10.029.

References

[1] I. Langmuir, The Role of Attractive and Repulsive Forces in the Formation of Tactoids, Thixotropic Gels, Protein Crystals and Coacervates, J. Chem. Phys. 6 (1938) 873–896.
[2] K. Norrish, Manner of Swelling of Montmorillonite, Nature 173 (1954) 256–257.
[3] R.M. Pashley, DLVO and Hydration Forces between Mica Surfaces in Li+, Na+, K+, and Cs+ Electrolyte Solutions: A Correlation of Double-Layer and Hydration Forces with Surface Cation Exchange Properties, J. Colloid Interf. Sci. 83 (1981) 531–546.
[4] J.N. Israelachvili, H. Wennerström, Role of Hydration and Water Structure in Biological and Colloidal Interactions, Nature 379 (1996) 219–225.
[5] A.D. Schlüter, J.P. Rabe, Dendronized Polymers: Synthesis, Characterization, Assembly at Interfaces, and Manipulation, Angew. Chemie Int. Ed. 39 (2000) 864–883.
[6] A. Delville, Beyond the Diffuse Layer Theory: A Molecular Analysis of the Structural, Dynamical, and Mechanical Properties of Charged Solid/Liquid Interfaces, J. Phys. Chem. C 117 (2013) 14558–14569.
[7] P.S. Low, Structure and Function of the Cytoplasmic Domain of Band 3: Center of Erythrocyte Membrane—Peripheral Protein Interactions, Biochim. Biophys. Acta (BBA)-Rev. Biomembr. 864 (1986) 145–167.
[8] R.M. Pashley, J.N. Israelachvili, Molecular Layering of Water in Thin Films between Mica Surfaces and Its Relation to Hydration Forces, J. Colloid Interf. Sci. 101 (1984) 511–523.
[9] G.C. Ansell, E. Dickinson, Sediment Formation by Brownian Dynamics Simulation: Effect of Colloidal and Hydrodynamic Interactions on the Sediment Structure, J. Chem. Phys. 85 (1986) 4079–4086.
[10] R. Aveyard, B.P. Binks, J.H. Clint, P.D. Fletcher, T.S. Horozov, B. Neumann, V.N. Paunov, J. Annesley, S.W. Botchway, D. Nees, et al., Measurement of Long-Range Repulsive Forces between Charged Particles at an Oil-Water Interface, Phys. Rev. Lett. 88 (2002) 246102.
[11] A. Prakash, D. Weygand, E. Bitzek, Influence of Grain Boundary Structure and Topology on the Plastic Deformation of Nanocrystalline Aluminum as Studied by Atomistic Simulations, Int. J. Plast. 97 (2017) 107–125.
[12] A.P. Lyubartsev, J.X. Tang, P.A. Janmey, L. Nordenskiöld, Electrostatically Induced Polyelectrolyte Association of Rodlike Virus Particles, Phys. Rev. Lett. 81 (1998) 5465–5468.
[13] R.H. French, V.A. Parsegian, R. Podgornik, R.F. Rajter, A. Jagota, J. Luo, D. Asthagiri, M.K. Chaudhury, Y.M. Chiang, S. Granick, et al., Long Range Interactions in Nanoscale Science, Rev. Mod. Phys. 82 (2010) 1887–1944.
[14] B.V. Deraguin, L. Landau, Theory of the Stability of Strongly Charged Lyophobic Sols and of the Adhesion of Strongly Charged Particles in Solution of Electrolytes, Acta Physicochim. USSR 14 (1941) 633–662.
[15] E.J.W. Verwey, J.T.G. Overbeek, K. Van Nes, Theory of the Stability of Lyophobic Colloids: The Interaction of Sol Particles Having an Electric Double Layer, Elsevier Publishing Company, 1948.
[16] J.P. Quirk, Soil Permeability in Relation to Sodicity and Salinity, Philos. Trans. R. Soc. London. Ser. A, Math. Phys. Sci. 316 (1986) 297–317.
[17] J.A. Greathouse, S.E. Feller, D.A. McQuarrie, The Modified Gouy-Chapman Theory: Comparisons between Electrical Double Layer Models of Clay Swelling, Langmuir 10 (1994) 2125–2130.
[18] W.B. Kleijn, J.D. Oster, A Model of Clay Swelling and Tactoid Formation, Clays Clay Miner. 30 (1982) 383–390.
[19] J.N. Israelachvili, R.M. Pashley, Molecular Layering of Water at Surfaces and Origin of Repulsive Hydration Forces, Nature 306 (1983) 249–250.
[20] M. Holmboe, S. Wold, M. Jonsson, Porosity Investigation of Compacted Bentonite Using XRD Profile Modeling, J. Contam. Hydrol. 128 (2012) 19–32.
[21] B. Gilbert, L.R. Comolli, R.M. Tinnacher, M. Kunz, J.F. Banfield, Formation and Restacking of Disordered Smectite Osmotic Hydrates, Clays Clay Miner. 63 (2015) 432–442.
[22] N. Güven, Molecular Aspects of Clay-Water Interactions, In: Clay-Water Interface and its Rheological Implications, Clay Mineral Society, Chapter 1 (1992).
[23] S.M. Acuña, P.G. Toledo, Nanoscale Repulsive Forces between Mica and Silica Surfaces in Aqueous Solutions, J. Colloid Interf. Sci. 361 (2011) 397–399.
[24] R. Kjellander, S. Marčelja, R.M. Pashley, J.P. Quirk, A Theoretical and Experimental Study of Forces between Charged Mica Surfaces in Aqueous CaCl2 Solutions, J. Chem. Phys. 92 (1990) 4399–4407.
[25] D. Grasso, K. Subramaniam, M. Butkus, K. Strevett, J. Bergendahl, A Review of Non-DLVO Interactions in Environmental Colloidal Systems, Rev. Environ. Sci. Biotechnol. 1 (2002) 17–38.
[26] V. Dahirel, M. Jardat, Effective Interactions between Charged Nanoparticles in Water: What Is Left from the DLVO Theory?, Curr Opin. Colloid Interface Sci. 15 (2010) 2–7.
[27] N.V. Churaev, Surface Forces in Wetting Films, Colloid Journal 65 (2003) 263–274.
[28] L. Liu, Prediction of Swelling Pressures of Different Types of Bentonite in Dilute Solutions, Colloids Surf. A 434 (2013) 303–318.
[29] V.E. Shubin, P. Kékicheff, Electrical Double Layer Structure Revisited via a Surface Force Apparatus: Mica Interfaces in Lithium Nitrate Solutions, J. Colloid Interf. Sci. 155 (1993) 108–123.
[30] J. Dziadkowiec, S. Javadi, J.E. Bratvold, O. Nilsen, A. Røyne, Surface Forces Apparatus Measurements of Interactions between Rough and Reactive Calcite Surfaces, Langmuir 34 (2018) 7248–7263.
[31] S.R. Van Lin, K.K. Grotz, I. Siretanu, N. Schwierz, F. Mugele, Ion-Specific and pH-Dependent Hydration of Mica-Electrolyte Interfaces, Langmuir 35 (2019) 5737–5745.
[32] I. Siretanu, D. Ebeling, M.P. Andersson, S.L.S. Stipp, A. Philipse, M.C. Stuart, D. Van Den Ende, F. Mugele, Direct Observation of Ionic Structure at Solid-Liquid Interfaces: A Deep Look into the Stern Layer, Sci. Rep. 4 (2014) 4956.
[33] S. Perkin, L. Crowhurst, H. Niedermeyer, T. Welton, A.M. Smith, N.N. Gosvami, Self-Assembly in the Electrical Double Layer of Ionic Liquids, Chem. Commun. 47 (2011) 6572–6574.
[34] A. Prakash, J. Pfaendtner, J. Chun, C.J. Mundy, Quantifying the Molecular-Scale Aqueous Response to the Mica Surface, J. Phys. Chem. C 121 (2017) 18496–18504.
[35] E.S. Boek, P.V. Coveney, N.T. Skipper, Monte Carlo Molecular Modeling Studies of Hydrated Li-, Na-, and K-Smectites: Understanding the Role of Potassium as a Clay Swelling Inhibitor, J. Am. Chem. Soc. 117 (1995) 12608–12617.
[36] C.L.G. Amorim, R.T. Lopes, R.C. Barroso, J.C. Querioz, D.B. Alves, C.A. Perez, H.R. Schelin, Effect of Clay-Water Interactions on Clay Swelling by X-Ray Diffraction, Nucl. Instruments Methods Phys. Res. Sect. A Accel. Spectrometers, Detect. Assoc. Equip. 580 (2007) 768–770.
[37] B. Jönsson, C. Labbez, B. Cabane, Interaction of Nanometric Clay Platelets, Langmuir 24 (2008) 11406–11413.
[38] M. Segad, B. Jönsson, T. Åkesson, B. Cabane, Ca/Na Montmorillonite: Structure, Forces and Swelling Properties, Langmuir 26 (2010) 5782–5790.
[39] L.J. Michot, I. Bihannic, F. Thomas, B.S. Lartiges, Y. Waldvogel, C. Caillet, J. Thieme, S.S. Funari, P. Levitz, Coagulation of Na-Montmorillonite by Inorganic Cations at Neutral pH. A Combined Transmission X-Ray Microscopy, Small Angle and Wide Angle X-Ray Scattering Study, Langmuir 29 (2013) 3500–3510.
[40] C.C. Tester, S. Aloni, B. Gilbert, J.F. Banfield, Short- and Long-Range Attractive Forces That Influence the Structure of Montmorillonite Osmotic Hydrates, Langmuir 32 (2016) 12039–12046.
[41] M. Ricci, P. Spijker, K. Voïtchovsky, Water-Induced Correlation between Single Ions Imaged at the Solid-Liquid Interface, Nat. Commun. 5 (2014) 4400.
[42] Z. Zachariah, R.M. Espinosa-Marzal, M.P. Heuberger, Ion Specific Hydration in Nano-Confined Electrical Double Layers, J. Colloid Interf. Sci. 506 (2017) 263–270.
[43] D. Li, J. Chun, D. Xiao, W. Zhou, H. Cai, L. Zhang, K.M. Rosso, C.J. Mundy, G.K. Schenter, J.J. De Yoreo, Trends in Mica-Mica Adhesion Reflect the Influence of Molecular Details on Long-Range Dispersion Forces Underlying Aggregation and Coalignment, Proc. Natl. Acad. Sci. 114 (2017) 7537–7542.
[44] D.J. Cebula, R.K. Thomas, S. Middleton, R.H. Ottewill, J.W. White, Neutron Diffraction From Clay-Water Systems, Clays Clay Miner. 27 (1979) 39–52.
[45] C.J. Van Oss, R.F. Giese, P.M. Costanzo, DLVO and Non-DLVO Interactions in Hectorite, Clays Clay Miner. 38 (1990) 151–159.
[46] E. Tombácz, T. Nyilas, Z. Libor, C. Csanaki, Surface Charge Heterogeneity and Aggregation of Clay Lamellae in Aqueous Suspensions, Prog. Colloid Polym. Sci. 125 (2004) 206–215.
[47] J. Wilson, J. Cuadros, G. Cressey, An in Situ Time-Resolved XRD-PSD Investigation into Na-Montmorillonite Interlayer and Particle Rearrangement during Dehydration, Clays Clay Miner. 52 (2004) 180–191.
[48] M. Dor, Y. Levi-Kalisman, R.J. Day-Stirrat, Y. Mishael, S. Emmanuel, Assembly of Clay Mineral Platelets, Tactoids, and Aggregates: Effect of Mineral Structure and Solution Salinity, J. Colloid Interf. Sci. 566 (2020) 163–170.
[49] M.L. Whittaker, L.N. Lammers, S. Carrero, B. Gilbert, J.F. Banfield, Ion Exchange Selectivity in Clay Is Controlled by Nanoscale Chemical-Mechanical Coupling, Proc. Natl. Acad. Sci. USA 116 (2019) 22052–22057.
[50] I.C. Bourg, J.B. Ajo-Franklin, Clay, Water, and Salt: Controls on the Permeability of Fine-Grained Sedimentary Rocks, Acc. Chem. Res. 50 (2017) 2067–2074.
[51] M.F. Hochella, D.W. Mogk, J. Ranville, I.C. Allen, G.W. Luther, L.C. Marr, B.P. McGrail, M. Murayama, N.P. Qafoku, K.M. Rosso, et al., Natural, Incidental, and Engineered Nanomaterials and Their Impacts on the Earth System, Science 363 (2019) eaau8299.
[52] M. Tuller, D. Or, Hydraulic Functions for Swelling Soils: Pore Scale Considerations, J. Hydrol. 272 (2003) 50–71.
[53] A. Revil, W.F. Woodruff, N. Lu, Constitutive Equations for Coupled Flows in Clay Materials, Water Resour. Res. 47 (2011) W05548.
[54] F.J. Carrillo, I.C. Bourg, C. Soulaine, Multiphase Flow Modelling in Multiscale Porous Media: An Open-Source Micro-Continuum Approach, J. Comput. Phys. X 8 (2020) 100073.
[55] D.A. Laird, Influence of Layer Charge on Swelling of Smectites, Appl. Clay Sci. 34 (2006) 74–87.
[56] E. Ferrage, Investigation of the Interlayer Organization of Water and Ions in Smectite from the Combined Use of Diffraction Experiments and Molecular Simulations. A Review of Methodology, Applications, and Perspectives., Clays Clay Miner. 64 (2016) 348–373.
[57] B. Ransom, H.C. Helgeson, A Chemical and Thermodynamic Model of Aluminous Dioctahedral 2: 1 Layer Clay Minerals in Diagenetic Processes; Regular Solution Representation of Interlayer Dehydration in Smectite, Am. J. Sci. 294 (1994) 449–484.
[58] D.A. Laird, C. Shang, Relationship between Cation Exchange Selectivity and Crystalline Swelling in Expanding 2:1 Phyllosilicates, Clays Clay Miner. 45 (1997) 681–689.

[59] T.A. Ho, J.A. Greathouse, Y. Wang, L.J. Criscenti, Atomistic Structure of Mineral Nano-Aggregates from Simulated Compaction and Dewatering, Sci. Rep. 7 (2017) 15286.
[60] X. Zhang, Z. Shen, J. Liu, S.N. Kerisit, M.E. Bowden, M.L. Sushko, J.J. De Yoreo, K. M. Rosso, Direction-Specific Interaction Forces Underlying Zinc Oxide Crystal Growth by Oriented Attachment, Nat. Commun. 8 (2017) 835.
[61] A. Cardellini, M. Alberghini, A.G. Rajan, R.P. Misra, D. Blankschtein, P. Asinari, Multi-Scale Approach for Modeling Stability, Aggregation, and Network Formation of Nanoparticles Suspended in Aqueous Solutions, Nanoscale 11 (2019) 3979–3992.
[62] H.D. Whitley, D.E. Smith, Free Energy, Energy, and Entropy of Swelling in Cs–, Na–, and Sr–Montmorillonite Clays, J. Chem. Phys. 120 (2004) 5387–5395.
[63] D. Ebrahimi, A.J. Whittle, R.J.-M. Pellenq, Mesoscale Properties of Clay Aggregates from Potential of Mean Force Representation of Interactions between Nanoplatelets, J. Chem. Phys. 140 (15) (2014) 154309.
[64] L. Sun, J.T. Hirvi, T. Schatz, S. Kasa, T.A. Pakkanen, Estimation of Montmorillonite Swelling Pressure: A Molecular Dynamics Approach, J. Phys. Chem. C 119 (2015) 19863–19868.
[65] D.E. Smith, Y. Wang, A. Chaturvedi, H.D. Whitley, Molecular Simulations of the Pressure, Temperature, and Chemical Potential Dependencies of Clay Swelling, J. Phys. Chem. B 110 (2006) 20046–20054.
[66] T.J. Tambach, P.G. Bolhuis, E.J.M. Hensen, B. Smit, Hysteresis in Clay Swelling Induced by Hydrogen Bonding: Accurate Prediction of Swelling States, Langmuir 22 (2006) 1223–1234.
[67] Y.-W. Hsiao, M. Hedström, Swelling Pressure in Systems with Na-Montmorillonite and Neutral Surfaces: A Molecular Dynamics Study, J. Phys. Chem. C 121 (2017) 26414–26423.
[68] T.R. Underwood, I.C. Bourg, Large-Scale Molecular Dynamics Simulation of the Dehydration of a Suspension of Smectite Clay Nanoparticles, J. Phys. Chem. C 124 (2020) 3702–3714.
[69] S. Plimpton, Fast Parallel Algorithms for Short-Range Molecular Dynamics, J. Comput. Phys. 117 (1995) 1–19.
[70] G. Fiorin, J. Hénin, A. Kohlmeyer, Collective Variables Module Reference Manual for LAMMPS, Albuquerque Sandia Natl Lab, 2013.
[71] G. Sposito, N.T. Skipper, R. Sutton, S.H. Park, A.K. Soper, J.A. Greathouse, Surface Geochemistry of the Clay Minerals, Proc. Natl. Acad. Sci. USA 96 (1999) 3358–3364.
[72] G.N. White, L.W. Zelazny, Analysis and Implications of the Edge Structure of Dioactahedral Phyllosilicates, Clays Clay Miner. 36 (1988) 141–146.
[73] L.N. Lammers, I.C. Bourg, M. Okumura, K. Kolluri, G. Sposito, M. Machida, Molecular Dynamics Simulations of Cesium Adsorption on Illite Nanoparticles, J. Colloid Interface Sci. 490 (2017) 608–620.
[74] C. Tournassat, J.A. Davis, C. Chiaberge, S. Grangeon, I.C. Bourg, Modeling the Acid-Base Properties of Montmorillonite Edge Surfaces, Environ. Sci. Technol. 50 (2016) 13436–13445.
[75] H.J.C. Berendsen, J.R. Grigera, T.P. Straatsma, The Missing Term in Effective Pair Potentials, J. Phys. Chem. 91 (1987) 6269–6271.
[76] R.T. Cygan, J.-J. Liang, A.G. Kalinichev, Molecular Models of Hydroxide, Oxyhydroxide, and Clay Phases and the Development of a General Force Field, J. Phys. Chem. B 108 (2004) 1255–1266.
[77] L.X. Dang, Mechanism and Thermodynamics of Ion Selectivity in Aqueous Solutions of 18-Crown-6 Ether: A Molecular Dynamics Study, J. Am. Chem. Soc. 117 (1995) 6954–6960.
[78] D.E. Smith, L.X. Dang, Computer Simulations of NaCl Association in Polarizable Water, J. Chem. Phys. 100 (1994) 3757–3766.
[79] J. Åqvist, Ion-Water Interaction Potentials Derived from Free Energy Perturbation Simulations, J. Phys. Chem. 94 (1990) 8021–8024.
[80] S. Gavryushov, P. Linse, Effective Interaction Potentials for Alkali and Alkaline Earth Metal Ions in SPC/E Water and Prediction of Mean Ion Activity Coefficients, J. Phys. Chem. B 110 (2006) 10878–10887.
[81] I.C. Bourg, G. Sposito, Connecting the Molecular Scale to the Continuum Scale for Diffusion Processes in Smectite-Rich Porous Media, Environ. Sci. Technol. 44 (2010) 2085–2091.
[82] E. Ferrage, B.A. Sakharov, L.J. Michot, A. Delville, A. Bauer, B. Lanson, S. Grangeon, G. Frapper, M. Jiménez-Ruiz, G.J. Cuello, Hydration Properties and Interlayer Organization of Water and Ions in Synthetic Na-Smectite with Tetrahedral Layer Charge. Part 2. Toward a Precise Coupling between Molecular Simulations and Diffraction Data, J. Phys. Chem. C 115 (2011) 1867–1881.
[83] A.A. Skelton, P. Fenter, J.D. Kubicki, D.J. Wesolowski, P.T. Cummings, Simulations of the Quartz(1011)/Water Interface: A Comparison of Classical Force Fields, Ab Initio Molecular Dynamics, and x-Ray Reflectivity Experiments, J. Phys. Chem. C 115 (2011) 2076–2088.
[84] M. Collin, S. Gin, B. Dazas, T. Mahadevan, J. Du, I.C. Bourg, Molecular Dynamics Simulations of Water Structure and Diffusion in a 1 nm Diameter Silica Nanopore as a Function of Surface Charge and Alkali Metal Counterion Identity, J. Phys. Chem. C. 122 (2018) 17764–17776.
[85] G. Gadikota, B. Dazas, G. Rother, M.C. Cheshire, I.C. Bourg, Hydrophobic Solvation of Gases (CO2, CH4, H2, Noble Gases) in Clay Interlayer Nanopores, J. Phys. Chem. C 121 (2017) 26539–26550.
[86] A. Laio, M. Parrinello, Escaping Free-Energy Minima, Proc. Natl. Acad. Sci. 99 (2002) 12562–12566.
[87] A. Laio, F.L. Gervasio, Metadynamics: A Method to Simulate Rare Events and Reconstruct the Free Energy in Biophysics, Chemistry and Material Science, Reports Prog. Phys. 71 (2008) 126601.
[88] B. Ensing, A. Laio, M. Parrinello, M.L. Klein, A Recipe for the Computation of the Free Energy Barrier and the Lowest Free Energy Path of Concerted Reactions, J. Phys. Chem. B 109 (2005) 6676–6687.
[89] M. Neumann, The Dielectric Constant of Water. Computer Simulations with the MCY Potential, J. Chem. Phys. 82 (1985) 5663–5672.
[90] J.L.F. Abascal, C. Vega, M. Neumann, A General Purpose Model for the Condensed Phases of Water: TIP4P/2005, J. Chem. Phys. 123 (2005) 234505.
[91] T.A. Ho, L.J. Criscenti, J.A. Greathouse, Revealing Transition States during the Hydration of Clay Minerals, J. Phys. Chem. Lett. 10 (2019) 3704–3709.
[92] J.A.R. Willemsen, S.C.B. Myneni, I.C. Bourg, Molecular Dynamics Simulations of the Adsorption of Phthalate Esters on Smectite Clay Surfaces, J. Phys. Chem. C 123 (2019) 13624–13636.
[93] P.E. Smith, W.F. van Gunsteren, Consistent Dielectric Properties of the Simple Point Charge and Extended Simple Point Charge Water Models at 277 and 300 K, J. Chem. Phys. 100 (1994) 3169–3174.
[94] M. Neumann, Dipole Moment Fluctuation Formulas in Computer Simulations of Polar Systems, Mol. Phys. 50 (1983) 841–858.
[95] H.W. Horn, W.C. Swope, J.W. Pitera, J.D. Madura, T.J. Dick, G.L. Hura, T. Head-Gordon, Development of an Improved Four-Site Water Model for Biomolecular Simulations: TIP4P-Ew, J. Chem. Phys. 120 (2004) 9665–9678.
[96] D. Van Der Spoel, P.J. Van Maaren, H.J.C. Berendsen, A Systematic Study of Water Models for Molecular Simulation: Derivation of Water Models Optimized for Use with a Reaction Field, J. Chem. Phys. 108 (1998) 10220–10230.
[97] S.W. De Leeuw, J.W. Perram, E.R. Smith, Simulation of Electrostatic Systems in Periodic Boundary Conditions. III. Further Theory and Applications, Proc. R. Soc. London, Ser. A 388 (1983) 177–193.
[98] I.C. Bourg, G. Sposito, A.C.M. Bourg, Modeling the Acid-Base Surface Chemistry of Montmorillonite, J. Colloid Interf. Sci. 312 (2007) 297–310.
[99] F.-R.C. Chang, G. Sposito, The Electrical Double Layer of a Disk-Shaped Clay Mineral Particle: Effect of Particle Size, J. Colloid Interf. Sci. 163 (1994) 19–27.
[100] F.-R.C. Chang, G. Sposito, The Electrical Double Layer of a Disk-Shaped Clay Mineral Particle: Effects of Electrolyte Properties and Surface Charge Density, J. Colloid Interf. Sci. 178 (2) (1996) 555–564.
[101] T.J. Tambach, Swelling of Clay Minerals, A Molecular Simulation Study, Ph.D. Thesis, University of Amsterdam, 2005 (2005).
[102] M. Holmboe, I.C. Bourg, Molecular Dynamics Simulations of Water and Sodium Diffusion in Smectite Interlayer Nanopores as a Function of Pore Size and Temperature, J. Phys. Chem. C 118 (2014) 1001–1013.
[103] D. Henderson, D. Boda, Insights from Theory and Simulation on the Electrical Double Layer, Phys. Chem. Chem. Phys. 11 (2009) 3822–3830.
[104] G. Sposito, The Surface Chemistry of Natural Particles, Oxford University Press, 2004.
[105] I.C. Bourg, G. Sposito, Molecular Dynamics Simulations of the Electrical Double Layer on Smectite Surfaces Contacting Concentrated Mixed Electrolyte (NaCl-CaCl2) Solutions, J. Colloid Interf. Sci. 360 (2011) 701–715.
[106] R.M. Tinnacher, M. Holmboe, C. Tournassat, I.C. Bourg, J.A. Davis, Ion Adsorption and Diffusion in Smectite: Molecular, Pore, and Continuum Scale Views, Geochim. Cosmochim. Acta 177 (2016) 130–149.
[107] P. Raiteri, R. Demichelis, J.D. Gale, M. Kellermeier, D. Gebauer, D. Quigley, L.B. Wright, T.R. Walsh, Exploring the Influence of Organic Species on Pre- and Post-Nucleation Calcium Carbonate, Faraday Discuss. 159 (2012) 61–85.
[108] N. Saiyouri, D. Tessier, P.Y. Hicher, Experimental Study of Swelling in Unsaturated Compacted Clays, Clay Miner. 39 (2004) 469–479.
[109] E. Ferrage, B. Lanson, B.A. Sakharov, V.A. Drits, Investigation of Smectite Hydration Properties by Modeling Experimental X-Ray Diffraction Patterns: Part I: Montmorillonite Hydration Properties, Am. Min. 90 (2005) 1358–1374.
[110] L.L. Schramm, J.C.T. Kwak, Influence of Exchangeable Cation Composition on the Size and Shape of Montmorillonite Particles in Dilute Suspension, Clays Clay Miner. 30 (1982) 40–48.
[111] G. Sposito, The Diffuse-Ion Swarm near Smectite Particles Suspended in 1: 1 Electrolyte Solutions: Modified Gouy-Chapman Theory and Quasicrystal Formation, In: Clay-Water Interface and its Rheological Implications, Clay Minerals Society, Chapter 3, 1992 (1992).
[112] R.M. Pashley, J.P. Quirk, The Effect of Cation Valency on DLVO and Hydration Forces between Macroscopic Sheets of Muscovite Mica in Relation to Clay Swelling, Colloids Surf. 9 (1984) 1–17.
[113] P.D. Svensson, S. Hansen, Combined Salt and Temperature Impact on Montmorillonite Hydration, Clays Clay Miner. 61 (2013) 328–341.
[114] M.V. Smalley, Electrical Theory of Clay Swelling, Langmuir 10 (1994) 2884–2891.
[115] I.S. Sogami, T. Shinohara, M.V. Smalley, Adiabatic Pair Potential of Highly Charged Plates in an Electrolyte, Mol. Phys. 76 (1992) 1–19.
[116] M.L. Sushko, K.M. Rosso, The Origin of Facet Selectivity and Alignment in Anatase TiO2 Nanoparticles in Electrolyte Solutions: Implications for Oriented Attachment in Metal Oxides, Nanoscale 8 (2016) 19714–19725.
[117] B.E. Novich, T.A. Ring, Colloid Stability of Clays Using Photon Correlation Spectroscopy, Clays Clay Miner. 32 (1984) 400–406.
[118] D.N. Petsev, P.G. Vekilov, Evidence for Non-DLVO Hydration Interactions in Solutions of the Protein Apoferritin, Phys. Rev. Lett. 84 (2000) 1339.
[119] M. Boström, D.R.M. Williams, B.W. Ninham, Specific Ion Effects: Why DLVO Theory Fails for Biology and Colloid Systems, Phys. Rev. Lett. 87 (2001) 168103.

[120] M.B. McBride, P. Baveye, Diffuse Double-Layer Models, Long-Range Forces, and Ordering in Clay Colloids, Soil Sci. Soc. Am. J. 66 (2002) 1207–1217.
[121] J.-P. Hansen, H. Löwen, Effective Interactions between Electric Double Layers, Annu. Rev. Phys. Chem. 51 (2000) 209–242.
[122] Y. Levin, Electrostatic Correlations: From Plasma to Biology, Reports Prog. Phys. 65 (2002) 1577–1632.
[123] A. Diehl, M.N. Tamashiro, M.C. Barbosa, Y. Levin, Density-Functional Theory for Attraction Between Like-Charged Plates, Physica A 274 (1999) 433–445.
[124] P.G. Kusalik, I.M. Svishchev, The Spatial Structure in Liquid Water, Science 265 (1994) 1219–1221.
[125] M.C.F. Wander, A.E. Clark, Structural and Dielectric Properties of Quartz - Water Interfaces, J. Phys. Chem. C 112 (2008) 19986–19994.
[126] S. Varghese, S.K. Kannam, J.S. Hansen, S.P. Sathian, Effect of Hydrogen Bonds on the Dielectric Properties of Interfacial Water, Langmuir 35 (2019) 8159–8166.
[127] C. Zhang, F. Gygi, G. Galli, Strongly Anisotropic Dielectric Relaxation of Water at the Nanoscale, J. Phys. Chem. Lett. 4 (2013) 2477–2481.
[128] L. Fumagalli, A. Esfandiar, R. Fabregas, S. Hu, P. Ares, A. Janardanan, Q. Yang, B. Radha, T. Taniguchi, K. Watanabe, et al., Anomalously Low Dielectric Constant of Confined Water, Science 360 (2018) 1339–1342.
[129] S. Perkin, R. Goldberg, L. Chai, N. Kampf, J. Klein, Dynamic Properties of Confined Hydration Layers, Faraday Discuss. 141 (2009) 399–413.
[130] U. Raviv, J. Klein, Fluidity of Bound Hydration Layers, Science 297 (2002) 1540–1543.
[131] G. Van Anders, D. Klotsa, N.K. Ahmed, M. Engel, S.C. Glotzer, Understanding Shape Entropy through Local Dense Packing, Proc. Natl. Acad. Sci. USA. 111 (2014) E4812–E4821.
[132] L. Onsager, The Effects of Shape on the Interaction of Colloidal Particles, Ann. N. Y. Acad. Sci. 51 (1949) 627–659.